 https://doi.org/10.3311/PPci.21569

Periodica Polytechnica Civil Engineering, 67(2), pp. 402–415, 2023

Accuracy Assessment of "Step-by-Step" Simulation Modeling Method for Rock Breaking by TBM Disc Cutters Assisted with Laser

Kui Zhang[1,2*], Minghai Kuang[2], Jingang Liu[2], Xuejun Zheng[2], Shuo Qiao[3]

[1] Postdoctoral Research Station for Mechanics, School of Mechanical Engineering and Mechanics, Xiangtan University, Xiangtan 411105, China
[2] Engineering Research Center of Complex Track Processing Technology & Equipment of Ministry of Education, Xiangtan 411105, China
[3] School of Mechanical and Electrical Engineering, Changsha University, Changsha 410022, China
* Corresponding author, e-mail: zhangk@xtu.edu.cn

Received: 21 November 2022, Accepted: 01 January 2023, Published online: 23 January 2023

Abstract

Rock breaking by laser-assisted disc cutters is a novel high-efficiency rock breaking mode that combines mechanical stress induced by the disc cutters with thermal cracking by laser. This paper presented a "step-by-step" simulation modeling concept, and conducted an in-depth study on potential influencing factors of simulation accuracy at each key step. First, the prediction accuracy of laser holes in laser drilling simulation was discussed. Second, the SHPB simulation and experiment were carried out to evaluate the accuracy of the selected material constitutive model in simulating the dynamic fracture damage of rock. Then, taking the laser-assisted rock-penetrating process of the scaled disc cutter as an example, the simulation prediction accuracy of rock-breaking by the disc cutter was analyzed. Finally, the simulation and experiment of laser-assisted disc cutter penetration into rock was carried out, and then the feasibility of the "step-by-step" concept was analyzed. The results show that: (1) in the laser drilling simulation, the predicted accuracy of laser hole size is higher when the power is low; with the laser power increases, the large amount of glass glaze will affect the subsequent modeling accuracy; (2) the HJC model can be used to simulate the transient nonlinear fracture damage behavior of granite; (3) the damage morphology of the granite obtained by the penetration simulation is highly similar to the experimental results, and the load curve should be corrected by the peak point fitting method. The results show the application prospects of the proposed numerical modeling method in future laser-assisted TBM tunnelling.

Keywords

"step-by-step" model, laser-assisted, simulation modeling, rock breaking, disc cutter

1 Introduction

In recent years, with the rapid increase in the demand for the development of underground space, a full-face rock tunnel boring machine (hereinafter referred to as TBM) is widely used in highway tunnels, railway tunnels, diversion tunnels, and other industries due to its advantages of high excavation efficiency and good safety, and low environmental impact, which has brought a widespread attention in TBM field [1–4].

During TBM excavation, under the combined action of the rotating torque of the cutterhead and the vertical thrust of the propulsion cylinder, the disc cutters mounted on the cutterhead penetrates into the rock, rotates and rolls to break the rock, forming a group of concentric circles on the tunnel face. However, when a TBM drives in adverse geological conditions such as "three highs" (high rock hardness, high confining pressure, and high quartz content), the damage and failure of TBM disc cutters are serious, which greatly affects the excavation efficiency, and rises the cost of construction. Therefore, it has become a topic of great significance to improve the rock- breaking ability of the disc cutter and prolong the service life of the tool.

In order to improve the tunneling efficiency in TBM excavation, researchers are trying to apply high-efficiency rock breaking technologies such as high-pressure water jet [5–6], microwave [7–8] and laser [9–10] to the TBM field. Among them, laser technology has relatively high

Cite this article as: Zhang, K., Kuang, M., Liu, J., Zheng, X., Qiao, S. "Accuracy Assessment of "Step-by-Step" Simulation Modeling Method for Rock Breaking by TBM Disc Cutters Assisted with Laser", Periodica Polytechnica Civil Engineering, 67(2), pp. 402–415, 2023. https://doi.org/10.3311/PPci.21569

application prospects in this field due to its outstanding advantages such as non-contact energy transmission, large heat transfer ratio, and high energy concentration [11]. For the prospective study of rock breaking by TBM disc cutters assisted with laser, physical experiment is undoubtedly one of the most rigorous and reliable methods to reveal the rock-breaking mechanism of laser-assisted TBM disc cutters [12]. However, due to the large size of the TBM cutterhead and the difficulty of sample preparation and installation, the experiments are risky and costly. In recent years, with the continuous development of numerical simulation techniques, appropriate visualization of the laser-assisted rock-breaking process of the disc cutters is expected not only to overcome the above limitations of the physical experiment, but also to gain insight into aspects which are not visible in reality. Due to the limitations of existing commercial simulation software, there are few reports on how to simulate rock-breaking process coupled with thermal cracking and mechanical crushing which are induced by laser and the tools, respectively. Fortunately, researchers have carried out a large number of studies in an attempt to model the rock-breaking process of laser and disc cutters, it can be summarized in brief as follows.

To understand the rock-breaking mechanism of the TBM disc cutter, numerous rock cutting simulations have been carried out using different cutting parameters, structure parameters, rock parameters, etc. In recent years, the existing research on numerical simulation of the rock-breaking process of the disc cutter under different working conditions can be separated into two broad categories based on their underlying theory: continuum-based methods and discrete methods [13]. Continuum-based methods include finite element methods (FEM), Eulerian methods, and smooth particle hydrodynamics (SPH) [14–16]. The results show that with the increase of the penetration depth, once the cutter spacing meets certain conditions, the lateral cracks initiating from the adjacent crushing zones expand gradually, and finally the rock between the adjacent concentric grooves collapses, resulting in massive rock debris which mainly affects the rock-breaking efficiency.

In the aspect of simulation research of laser breaking rock, based on the thermodynamic theory, the damage evolution process of rock during laser irradiation is investigated by simulation [17–20]. The purpose of this investigation is to explore the influence of laser parameters on the rock damage morphology, changes in temperature field, and the weakening degree of the rock strength, so as to analyze the breaking-rock mechanism of laser. The formation process of rock surface cracks under laser irradiation can be divided into four stages: heat transfer, generation of stresses, melting and solidification, vaporization, and phase explosion [21]. Initially, the temperature of rock increases gradually, but when it does not beyond its melting point, the crushing method of the rock is mainly thermal crushing, and the crushed debris can be blown away by the assist gas flow. Then the temperature in the irradiation zone rises sharply to the melting point of the rock, and the rock begins to melt. And a small amount of bubbles appear in the molten pool, due to the escape of the sealed gases in the original pores and the thermally decomposed gases of special mineral components (such as silicate, etc.) [22]. With the continuous irradiation of the laser, the temperature continues to rise and the molten pool gradually boils; the number of bubbles increases, and the bubbles constantly grow until they burst. Since the melt and vapor can not be timely blown away by the assist gas flow, they will resolidify into glass glaze on the surface of the drilling hole. The resulting glass glaze will hinder the propagation of the laser beam energy to the deeper rock mass, thus affecting the efficiency of laser rock breaking.

The above research will help the academic community to deeply understand the rock-breaking mechanism of disc cutters and laser. On this basis, in order to overcome the aforementioned limitations of the physical experiment and the existing commercial simulation software, this paper firstly proposed an economical "step-by-step" simulation modeling concept of laser-assisted rock breaking of the disc cutters. Secondly, in each step, the influencing factors of the simulation modeling accuracy were discussed, and the setting of the key simulation modeling parameters was analyzed. Thirdly, taking the laser-assisted rock-penetrating process of the scaled disc cutter as an example, the key modeling parameters were properly set on the basis of fully considering the influencing factors; and then, the numerical modeling for the study case was carried out using the "step-by-step" method. Finally, experimental research was also conducted to preliminarily verify the feasibility of the proposed modeling concept.

2 Rock-breaking mode of laser-assisted disc cutters and its numerical modeling concept

2.1 Rock-breaking mode of laser-assisted disc cutters

Based on the understanding of the rock-breaking mechanism of the cutters and laser, a novel rock-breaking mode of TBM disc cutters is proposed as shown in Fig. 1. Compared with the traditional rock-breaking mode of the

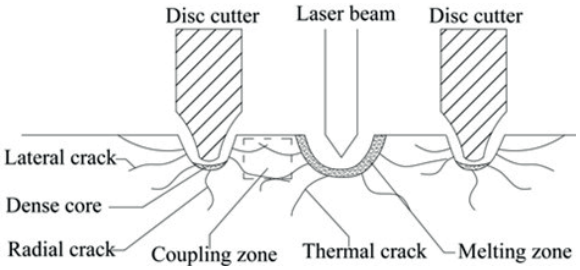

Fig. 1 Schematic diagram of rock breaking by cutters assisted with laser

disc cutters, in this new mode, the laser transmitted module mounted on the cutterhead can emit laser which radiates the rock between the adjacent disc cutters, producing laser-induced rock damage such as thermal cracks before mechanical crushing by the cutters. The following are the expected benefits of this new mode:

1. the laser is used to form cracks and holes in the rock, thereby destroying the integrity of the rock and weakening the strength of the rock;
2. the thermal-mechanical coupling effect will promote the intersection of thermal and lateral cracks, thereby improving the rock-breaking efficiency of the cutters.

2.2 "Step-by-step" simulation modeling concept

A "step-by-step" simulation modeling concept is proposed. The numerical modeling concept typically involves the following key steps:

S1: based on the principle of thermodynamics and the life-death element method, a numerical model of laser rock breaking is established in ANSYS to predict the morphology of thermal damage (such as cracks, holes, cuts, etc.).

S2: according to the damage morphology obtained in S1, a FE model of rock with multiple replicated thermal damage is reconstructed in a multi-disciplinary FE preprocessor (such as HyperMesh). For example, assume that only laser-induced holes are considered, the holes with the same profile shape, the given number of holes, the given hole-hole distance and cutter-hole distance can be replicated in the FE model of rock.

S3: considering that the tool-rock interaction process is a typical nonlinear transient event, the FE model of rock reconstructed in S2 is imported into a transient dynamic nonlinear finite element program (such as LS-DYNA, Abaqus, Nastran, etc.) and then a computational material model for describing the dynamic constitutive behaviors of rock (such as Holmquist-Johnson-Cook model, Johnson-Holmquist-Ceramic model, Riedel-Hiermaier-Thoma model, etc.) is reasonably selected. By introducing the FE model of the cutters into the rock model, the nonlinear model of rock breaking by the disc cutters is finally established, which is used to indirectly simulating the laser-assisted rock-breaking process of the disc cutters.

2.3 Analysis of potential influencing factors of simulation modeling accuracy

Factors at each step which may have a potential influence on the overall accuracy of the "step-by-step" simulation modeling concept are briefly discussed below:

1. the prediction accuracy of laser rock breaking simulation in S1, i.e., whether the numerical model of laser rock breaking can effectively predict the morphology of the laser-induced damage.
2. the simulation accuracy of the material constitutive model in S2, i.e., whether the selected rock computational model can accurately describe the dynamic constitutive behaviors of the rock samples subjected to the cutting load.
3. the simulation accuracy of rock breaking by the disc cutters, i.e., whether the nonlinear model can effectively reveal the coupling rock-breaking mechanism and well predict the internal damage state associated with progressive rock failure due to the dynamic disturbance of the disc cutters and the pre-irradiation of laser.

It is necessary to conduct in-depth studies on the above potential influencing factors before modeling.

3 Accuracy analysis of laser rock-breaking simulation in S1

For reasons of space, taking laser drilling as an example, the simulation accuracy of laser rock breaking is discussed in this section.

3.1 Laser drilling modeling and simulation analysis

Assuming that the laser heat source follows the Gaussian distribution model [23], the thermodynamics-based FE model of laser drilling was established using ANSYS Parametric Design Language command flow (APDL). The thermophysical and mechanical parameters of rock are listed in Table 1. The laser drilling process was simulated using element birth and death technique which can define the "birth" and "death" times for a specific set of elements. More specifically, in this simulation analysis, the elements of rock were all defined as live ones at the first time; when the temperature of the element exceeds the melting point of rock, or the thermal stress of the element exceeds the rock strength, the rock element will be automatically "killed"

Table 1 Thermophysical and mechanical parameters of granite

Thermophysical parameters		Mechanical parameters	
Specific heat capacity (kJ/kg·K)	750	Uniaxial compressive strength (MPa)	123.3
Thermal conductivity (W/(m·K))	4.4	Uniaxial tensile strength (MPa)	5.69
Melting point (°C)	1400	Density (kg/m^3)	2700
Linear expansion coefficient	5.6×10^{-6}	Elastic modulus (GPa)	210

by the program. The laser power range was set from 10 W to 100 W, the diameter of the laser beam was set to 1 mm, the irradiation angle was set to 90°, and the time step was set to 0.01 s. There were 10 steps in total.

Fig. 2 illustrates cross-sectional views of the rock samples under different powers obtained by the laser drilling simulation. It shows that the failure morphology of the rock samples has an "inverted cone" shape, and its size increases with the increase of laser power. The Gaussian distribution of the laser heat source is the main reason for this failure morphology. More specifically, the temperature of the rock elements irradiated by the central region of the laser beam that have the highest energy rises fastest and therefore these elements will be deleted first. The hole wall absorbs less energy from the edge of the laser beam, causing the temperature rise rate of the hole wall is much lower than the hole bottom, so the hole diameter increases at a slower rate than the hole depth.

3.2 Laser-drilling experiment and accuracy analysis

(1) *Test apparatus and specimen preparation*

As shown in Fig. 3(a), E1309M high-speed precision laser cutting machine was selected as the laser drilling test platform. As shown in Fig. 3(b), granite samples with a size of 300 mm × 200 mm × 80 mm were selected, and its thermophysical and mechanical parameters are shown in Table 1.

(2) *Experimental procedure*

In order to reliably evaluate the prediction accuracy of the laser drilling simulation described above, the experiment was repeated under similar conditions using the same laser cutting parameters (as the simulation). During the experiment, the assist gas flow was used to blow away the rock debris and melts. After irradiation, the damage profile of each rock sample was carefully observed, meanwhile the average laser aperture and hole depth were measured.

(3) *Accuracy analysis*

Fig. 4 shows the hole morphology obtained by the laser drilling tests. Comparing Fig. 2 and Fig. 4 shows that the

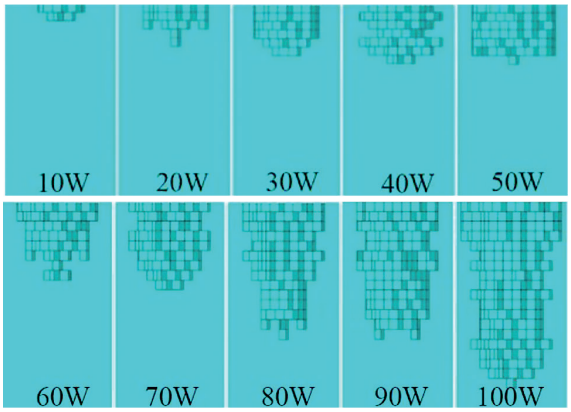

Fig. 2 Cross-sectional views of the rock samples under different powers

(a) (b)

Fig. 3 (a) High-speed precision laser cutting machine and (b) rock samples

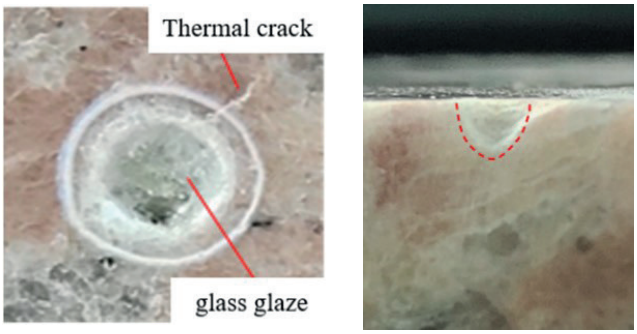

(a) (b)

Fig. 4 Morphology of holes obtained by the laser drilling tests: (a) thermal crack and glass glaze; (b) cross-sectional topography

predicted morphology of laser holes is consistent with the experimental observation. Since some lava accumulated on the lase hole bottom at a certain hole depth cannot be blown out by the assist gas flow, it will eventually solidify into the glass glaze on the hole wall. Due to the limitations of the birth-death element method, it could be impossible to simulate the formation process of the glass glaze. Therefore, it could be difficult to take into account the influence of this material on the simulation results, such as the repeated absorption of laser beam energy and the inhibition of energy transfer.

Fig. 5 is a graph of the diameter and depth of the laser holes obtained by the simulation and the experiment as a function of laser power. It can be seen from the figure that:

1. the variation trend of the diameter/depth with the laser power obtained by the simulation is roughly the same as that by the experiment; with the increase of the laser power, the hole size generally increases.
2. when the laser power does not exceed 90 W, the prediction accuracy of the hole diameter is higher than when the power exceeds 90 W. For example, when the laser power is 100 W, the diameter predicted by the simulation is obviously larger than by the experiment.
3. when the laser power does not exceed 70 W, the simulation prediction accuracy of the hole depth is higher than when the power exceeds 70 W. For example, when the laser power is 80 W, the depth predicted by the simulation is obviously larger than by the experiment.

There exists an obvious deviation between the actual hole size and the predicted value when the laser power is set too large (e.g., 100 W). The reason is that the glass glaze produced in large quantities under the high laser power will hinder the transmission efficiency of the laser energy and therefore slow down the increase rate of the hole size.

In summary, the simulated laser hole morphology is consistent with the experimental results, and both of them have an "inverted cone" shape. When the laser power does not exceed 70 W, the simulation prediction accuracy of the hole size is higher than when the power exceeds 70 W. Among them, the simulation prediction accuracy of the hole diameter is higher than that of the hole depth. However, the simulation cannot simulate the formation process of the glass glaze and its influence on the energy transfer and distribution, resulting in poor simulation accuracy under high laser power. In engineering applications, considering that the laser power required is high, the influence of glass glaze on the simulation prediction accuracy cannot be ignored (especially when predicting the hole depth), so the simulation results of laser drilling should be corrected.

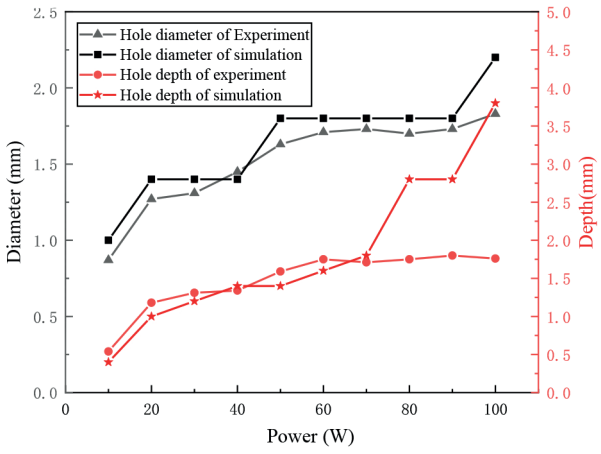

Fig. 5 Comparison of the diameter and depth of the laser holes obtained by the simulation and the experiment

4 Accuracy analysis of rock constitutive model in S2

Material constitutive model is one of the basic scientific fundamentals for simulation accuracy of rock breaking. The rock constitutive model in this simulation should be properly selected based on the knowledge of the rock breaking mechanism of the tools. According to the existing research, it is known that when the disc cutters break rock, on the one hand, the complex nonlinear contact behavior occurs on the interface between the cutters and rock, and on the other hand, deformation, damage accumulation and transient fracture behavior occur inside the rock mass. Since Holmquist-Johnson-Cook elastoplastic constitutive model (hereinafter referred to as HJC model) performs well in simulating similar problems such as rock deformation behavior at high strain rates and concrete failure behavior under impact load [24–25], theoretically it could be applied to simulate rock-breaking process of disc cutters. Impact tests are normally used to study dynamic deformation and failure modes of materials. In order to validate the accuracy of the HJC model in simulating rock-breaking process of disc cutters, numerical simulation of Split-Hopkinson Pressure Bar (SHPB) Tests was performed in ANSYS/LS-DYNA, where high and low impact velocities were selected to approximately reflect the rock-breaking velocity level of the disc cutters.

4.1 HJC model

In the HJC model, the normalized equivalent stress σ^* is defined as follows [26]:

$$\sigma^* = \left[A(1-D)+BP^{nN}\right]\left[1+c\ln\left(\dot{\varepsilon}^*\right)\right], \tag{1}$$

$$P^n = P / f_c', \tag{2}$$

$$\dot{\varepsilon}^* = \dot{\varepsilon}/\dot{\varepsilon}_0. \tag{3}$$

Where D $(0 \le D \le 1)$ is the damage variable; P is the actual pressure; P^n is the normalized pressure; f_c' is the quasi-static uniaxial compressive strength; $\dot{\varepsilon}^*$ is the dimensionless strain rate; $\dot{\varepsilon}$ is the actual strain rate; $\dot{\varepsilon}_0$ is

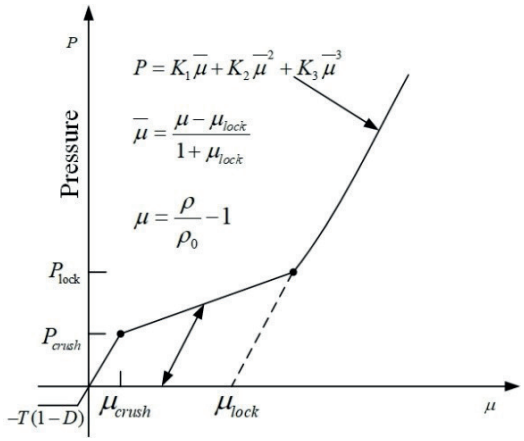

Fig. 6 Pressure-volume responses of the HJC damage model

the reference strain rate; A is the normalized cohesive strength; B is the normalized pressure hardening coefficient; c is the strain rate coefficient; N is the pressure hardening exponent.

The HJC model can be considered a strain-based damage model, in which the damage variable D is calculated from both the equivalent plastic strain increment $\Delta\varepsilon_p$, and the equivalent plastic volumetric strain increment $\Delta\mu_p$, so the damage variable D is written as follows:

$$D = \sum \frac{\Delta\varepsilon_P + \Delta\mu_P}{D_1\left(P'' + T''\right)^{D_2}}, \tag{4}$$

$$T'' = T / f_c', \tag{5}$$

where T, T'' and D_1 (D_2) are the maximum static tension, the maximum static pressure and the damage constant of the material, respectively.

The pressure-volume behaviors of the HJC model can be expressed by three regions, as shown in Fig. 6. The first part is linear elastic from the negative pressure cutoff $-T(1-D)$ to the elastic limit P_{crush}. The second part is the plastic strain stage. In this stage, the air voids are gradually compressed out of the rock, resulting in the occurrence of plastic volumetric strain. At the end of this stage, it is assumed that the rock material is totally damaged without tensile strength and then compacted. In the third stage, the fully dense material without any air voids is defined, and the pressure-volume responses at this region are expressed as:

$$P = K_1\bar{\mu} + K_2\bar{\mu}^2 + K_2\bar{\mu}^3, \tag{6}$$

where K_1, K_2 and K_3 are the rock material constants; $\bar{\mu}$ is the modified volumetric strain.

4.2 SHPB modeling and simulation analysis

Three-dimensional (3D) numerical model of SHPB was established using explicit finite element method for nonlinear transient dynamics in ANSYS/LS-DYNA. Both bars (i.e., strike bar, incident bar and transmitted bar) and the granite specimen were discretized with SOLID 64 3D solid elements. The incident bar and transmitted bar are made of steel, and they were described by the elastic constitutive model. Their characteristic parameters are shown in Table 2. The specimen, strike bar, incident bar and transmitted bar have the same diameter of 40 mm, while their lengths are 25 mm, 300 mm, 2000 mm and 2000 mm, respectively. The parameters of HJC model for granite are shown in Table 3 [27–28].

The incident compressive wave for the simulation is applied on the incident bar as the only load boundary condition to replace the impacting effect of the striker. The keyword "Automatic_Surface_to_Surface" is used to describe the contact between the specimen bar and pressure bar to avoid interpenetration. In addition, viscous hourglass control is applied to the entire numerical model. The time step factor is defined as 0.6 in the current simulation to ensure convergence. The keyword "Initial_Velocity" is adopted to generate various velocities for the strike bar.

In order to reasonably evaluate the simulation accuracy of rock constitutive behavior, the range of the impact velocity in the SHPB simulation should match the rock breaking velocity of the disc cutter. Taking the existing

Table 2 Characteristic parameters of incident bar and transmitted bar

Density(kg/m^3)	Elasticity modulus E(GPa)	Poisson's ratio μ
7830	210	0.3

Table 3 Parameters of HJC model for granite

ρ/kg/m^3	G/GPa	A	B	c	N	f_c'/MPa	T/MPa	S_{max}	EF_{min}
2700	4.58	0.279	1.60	0.007	0.61	123.3	5.69	7.0	0.01
P_{crush}/MPa	u_{crush}	P_{lock}/MPa	u_{lock}	D_1	D_2	K_1/GPa	K_2/GPa	K_3/GPa	F_S
10.0	0.001	800	0.1	0.04	1.0	85	-171	208	-1

Notes: ρ is rock density; G is shear modulus; P_{crush} is crush pressure; u_{crush} is crush volumetric strain; P_{lock} and u_{lock} are the pressure and the corresponding volumetric strain, respectively, when all air voids are removed from the rock material; S_{max} is the maximum dimensionless strength coefficient; EF_{min} is the damage parameter; F_S is rock failure types.

large-diameter TBM "Caucasus" as an example, the maximum linear velocity of the disc cutter can be as high as 8 m/s. In the future, with the increase of diameter and rotating speed of the cutterhead, the maximum cutting velocity of the disc cutter is expected to double. In view of this, the impact velocity in the simulation was set to 8 and 16 m/s, which represents the maximum cutting velocity of the existing and future TBM, respectively. Fig. 7 shows the transfer process of stress wave in the specimen obtained by SHPB simulation. It can be seen from the figure that when the striker bar is launched towards the incident bar, a compressive stress wave (incident wave) will be generated, and then the incident wave will propagate to the rock sample along the axis of the incident bar. Once the incident wave reaches the interface between the incident bar and the rock sample, a portion of the incident wave will be reflected back into the incident bar, known as the reflected wave; in the meantime, the remaining incident wave will pass through the rock sample and then be transmitted to the transmitted bar, which is referred to as the transmitted wave. The incident and reflected waves are recorded by a history node located in the incident bar; the transmitted waves are recorded by a history node located in the transmitted bar.

The stress $\sigma(t)$, strain $\varepsilon(t)$, and strain rate $\dot{\varepsilon}(t)$ of the rock sample in SHPB numerical simulation can be calculated by the following formula [29]:

$$\sigma(t)=\frac{A_1}{2A_0}E\left(\varepsilon_{\mathrm{I}}+\varepsilon_{\mathrm{R}}+\varepsilon_{\mathrm{T}}\right), \tag{7}$$

$$\varepsilon(t)=\frac{C_0}{L_0}\int_0^t\left(\varepsilon_{\mathrm{I}}-\varepsilon_{\mathrm{R}}-\varepsilon_{\mathrm{T}}\right)\mathrm{d}t, \tag{8}$$

$$\dot{\varepsilon}(t)=\frac{C_0}{L_0}\left(\varepsilon_{\mathrm{I}}-\varepsilon_{\mathrm{R}}-\varepsilon_{\mathrm{T}}\right), \tag{9}$$

where A_0 and A_1 are the cross-sectional area of the rock sample and the pressure bar, respectively; ε_I, ε_R, ε_T are the incident wave signal, reflected wave signal and transmitted wave signal measured by the strain gauges, respectively; C_0 is the wave velocity of the pressure bar.

4.3 SHPB experiment and accuracy analysis

(1) *Experimental procedure*

Fig. 8 is the experimental installation of SHPB. The material parameters are the same as the SHPB numerical model. Since granite is a non-homogeneous brittle material which is sensitive to strain rate, it is necessary to paste a brass sheet at the center of the impacted part of the incident bar

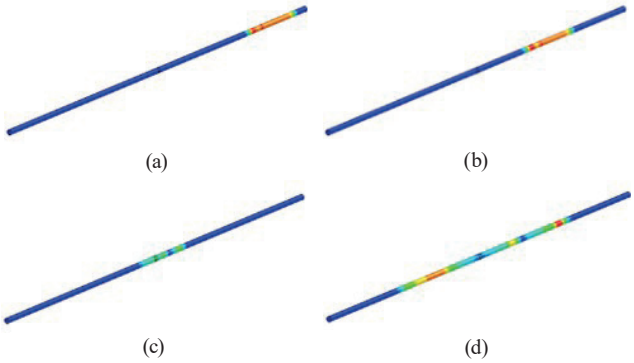

Fig. 7 Transfer process of stress wave in the specimen obtained by SHPB simulation: (a) the initial stage of stress wave generation; (b) the stress wave is transmitted to the incident bar; (c) the stress wave is transmitted to the rock; (d) the stress wave is transmitted back to the incident bar

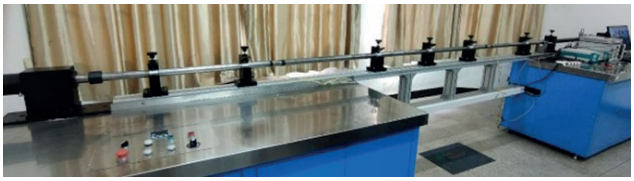

Fig. 8 Experimental installation of SHPB

to absorb the energy brought by the impact bar and reduce the high-frequency oscillation of the incident wave. Apply grease evenly to the circular surfaces at both ends of the specimen to reduce the end effect of the contact surface between the pressure bar and the specimen, then, sandwich the granite specimen between the incident bar and the transmitted bar to ensure that the pressure bar, the specimen and the impact bar have coincident axes.

(2) *Simulation accuracy analysis of rock constitutive behavior*

Fig. 9 shows the stress-strain curves obtained by SHPB simulation and experiment. It can be seen from the figure:

1. when the initial impact velocity is set to 8 m/s, the simulated stress-strain curve in the elastic-plastic deformation stage illustrates a good agreement with the experimental results. The variation of stress-strain prediction accuracy at the late plastic stage and the failure stage of the specimen satisfying engineering accuracy. The error of the peak stress predicted by the simulation relative to the experimental value (103.15 Mpa) is 11.15%.
2. when the initial impact velocity is set to 16 m/s, the simulated stress-strain curve in the elastic stage illustrates a good agreement with the experimental results. However, the error of the predicted peak stress (237.19 Mpa) obtained at the plastic stage and

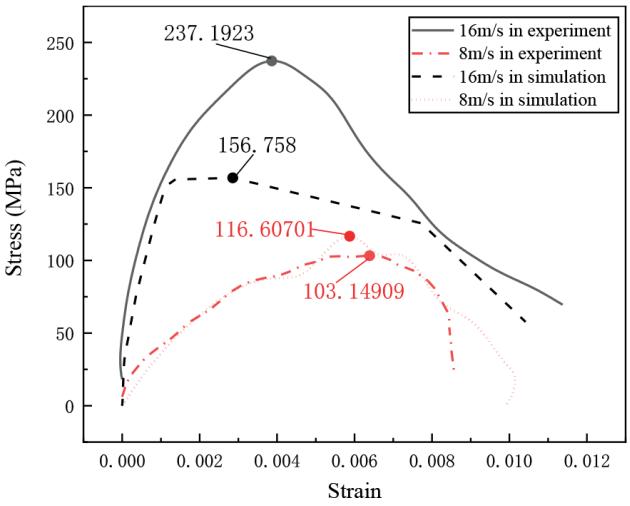

Fig. 9 Stress-strain curves obtained by SHPB simulation and experiment

the failure stage of the specimen is 33.91% (relative to the experimental value); the simulation accuracy is significantly reduced due to the following reasons: on the one hand, the selected rock constitutive model is a homogeneous material model, while the granite sample is actually a non-homogeneous material, and there are material defects such as crack damage; on the other hand, there is a systematic measurement error in the SHPB experiment device.

Fig. 10 shows that the macroscopic failure characteristics of the real rock specimen and the numerical specimen are similar when the initial impact velocity is set to 8 m/s. The cracks originating from the middle of the granite sample spread to the surrounding, resulting in large rock debris.

In summary, the HJC model can accurately simulate the transient nonlinear fracture behavior of the rock under the action of the existing TBM disc cutters within the given impact velocity range. However, when dealing with the modeling needs for high-speed rock breaking by super-large-diameter cutterheads in the future, the HJC model should be properly revised to improve the simulation accuracy.

5 Accuracy analysis of disc cutter rock-breaking simulation in S3

Accuracy analysis of S3 was also conducted by comparing the results obtained by disc cutter rock-breaking simulation and experiment. Considering the huge size of the actual disc cutter, the time-consuming and laborious operation, in order to reduce the difficulty of the experiment

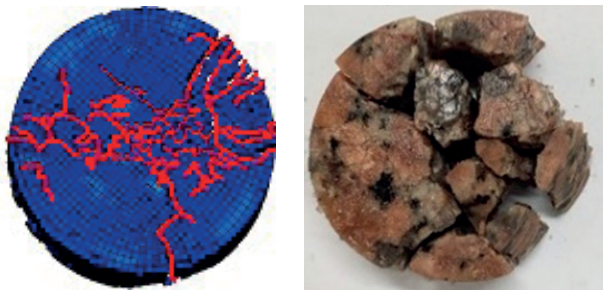

(a) (b)

Fig. 10 The failure morphology of granite sample obtained by (a) SHPB simulation and (b) experiment

and simulation time, the rock-cutting process by the disc cutter is simplified as the rock penetration by a reduced-scale disc cutter.

5.1 rock-penetration modeling and simulation analysis

(1) *Model setup*

As shown in Fig. 11, a FE model of rock penetration by a flat-edged constant-section cutter ring is established. The dimension ratio of the cutter ring to the 17-inch engineering cutter was 1:3. The Blade width and blade angle of the scaled cutter ring was 3 mm and 8°, respectively. The simplification process of the disc cutter is shown in Fig. 12. The size of the rock model was 124 mm × 33 mm × 9mm. The elements within the "cross-shaped" zone of the rock facing the cutter ring were refined with the mesh size of 0.2 mm. To create a smoother model, the remaining zone was automatically meshed in an adaptive meshing increment. The cutter ring and rock sample were defined as the rigid body and HJC model, respectively. The physical and mechanical parameter settings of the cutter ring are also shown in Table 2.

The cutter-rock contact was defined as face-to-face eroding contact. The outer surface of the cutter ring was set as the master contact surface, and the rock surface was set as the slave contact surface. The static and dynamic friction coefficients between the two surfaces was set to

Fig. 11 FE model of rock penetration by the cutter ring

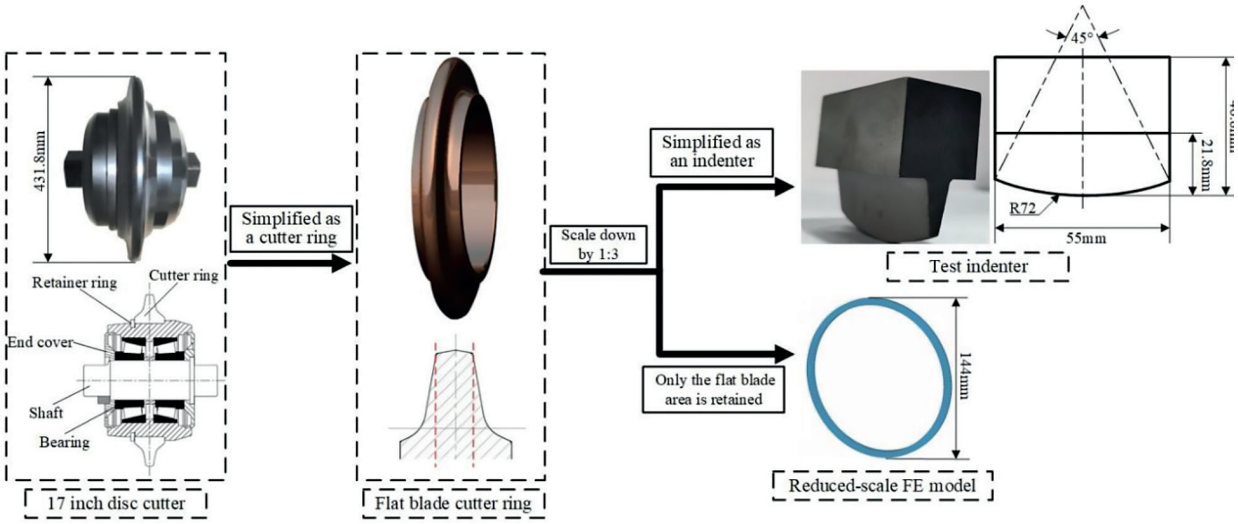

Fig. 12 The simplification process of the disc cutter

0.2 and 0.1, respectively. In order to eliminate the boundary effect, the non-reflection boundary condition was set on the rock surfaces except the contact surface of the cutter and rock. Only the penetration movement of the ring was allowed. The bottom surface of the rock was loaded by a fixed boundary.

(2) *Simulation analysis*

Fig. 13 shows the damage morphology of the rock surface obtained by the simulation. It can be seen from the figure that once the stress state of a rock element reaches the critical value defined by the HJC model, the element is deleted, thereby forming an "indentation"; with increase of the penetration depth, the size of the "indentation" continues to expand, further forming a cutting groove which is directly below the cutter edge.

As the TBM disc cutter penetrates the rock, the rolling force and lateral force of the cutter are very small. The accuracy of the penetration model is determined by comparing the prediction accuracy of the vertical force.

The predicted results of the penetration depth-vertical force curve are shown in Fig. 14. It shows that as the penetration depth increases, the vertical force of the cutter ring shows an increasing trend. At the initial stage of penetration, the vertical force increases with the increase of penetration depth. When the penetration depth increases to a certain value, the vertical force drops abruptly, and the cutter ring begins to unload. The main reason is that when the force on the rock exerted by the cutter exceeded the failure strength, the rock elements fail and are stripped from the parent body. When the stripped rock element reaches a certain value, it causes the "void" phenomenon of the cutter, the disc cutter force drops sharply, and

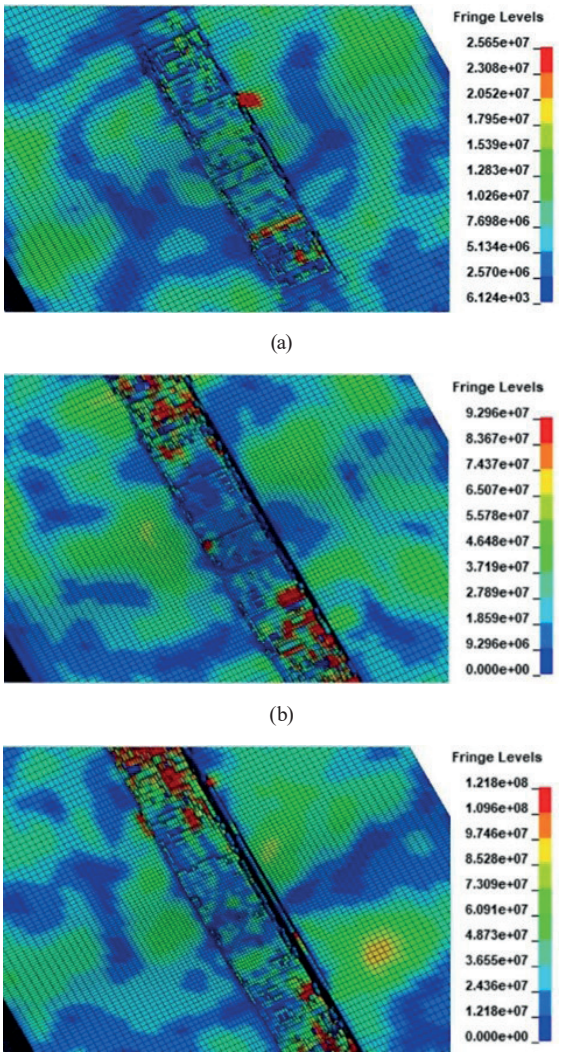

Fig. 13 Morphology of rock samples obtained by the simulation (a) Penetration depth 1 mm, (b) Penetration depth 2 mm, (c) Penetration depth 3 mm

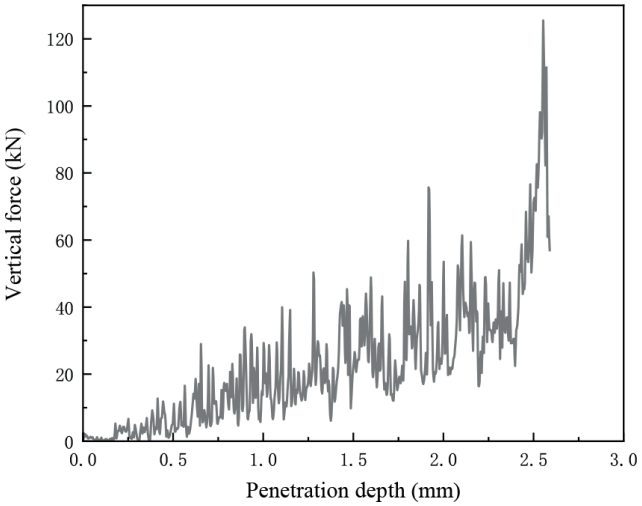

Fig. 14 The penetration depth-vertical force curve obtained by the simulation

a "leap forward" fracture of the rock occurs. With the continuous penetration of the cutter, the contact area between the disc cutter and the rock gradually increases; once the full-width contact is reached, and another large collapse occurs. Therefore, the process of the disc cutter penetrating into the rock is a continuous cycle composed of several small collapses and one large collapse, which leads to the leap forward crushing of the rock under the action of the disc cutter, and the vertical force is fluctuating up and down during the penetration process.

5.2 Penetration experiment and accuracy analysis

(1) *Experimental procedure*

As shown in Fig. 15, the CMT5105 microcomputer-controlled electronic universal testing machine was used as the penetration experiment platform. In order to work better with the testing machine, one-eighth of the scaled cutter used in the simulation was selected as the experimental indenter (corresponding to a central angle of 45° (Fig. 12).

(2) A*nalysis of simulation accuracy of rock breaking by disc cutter*

The morphology of the rock surface obtained by the penetration tests is shown in Fig. 16. Comparing Fig. 13 and Fig. 16, it can be seen that the geometric shapes and sizes of indentations predicted by the penetration simulation are basically consistent with the experiment results. The difference is that the failed rock underneath the blade will be break into rock powder and then further squeezed into a dense core under the confinement of the surrounding rock mass, instead of being directly deleted in the simulation. Due to the limitations of finite element technology, the dynamic derivation process of the dense core could not

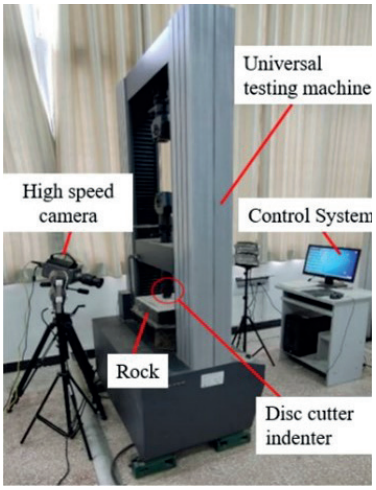

Fig. 15 Test system used for the penetration tests

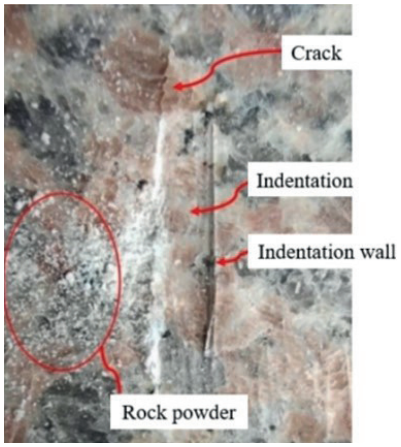

Fig. 16 Failure morphology of granite samples obtained by the penetration experiment

be simulated, and therefore it is almost impossible to take into account its impact on the rock-breaking mechanism of TBM cutters.

The experiment was conducted three times to obtain the average vertical force to reduce random errors and eliminate the instability caused by manual operation. As shown in Fig. 17, the vertical force vs. penetration depth curves which are indexed as L1~L3 come from three repeated experiments; the average vertical force vs. penetration depth curve is indexed as L.

Fig. 18 shows the variation of vertical force with penetration depth obtained by simulation and experiment. As shown in Fig. 18, the peak point line M1 is a polyline which is connected by peak points selected in a monotonically increasing manner from the simulated curve M; the peak fitted curve M2 is obtained by fitting the peak point line M (known as the peak point fitting method); the mean fitted curve M3 is obtained by fitting the simulated

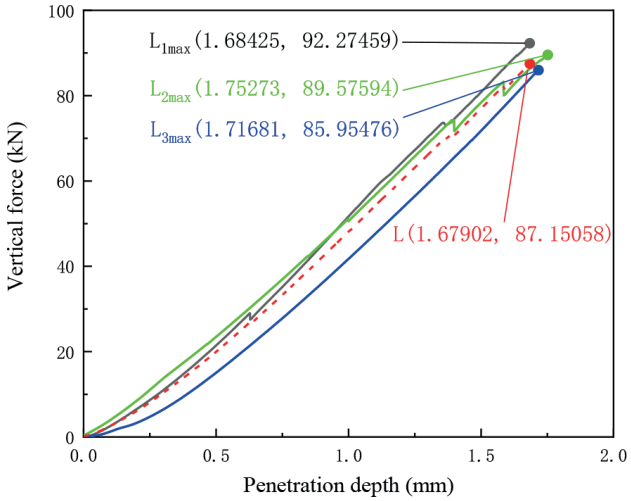

Fig. 17 The penetration depth-vertical force curve obtained by the experiment

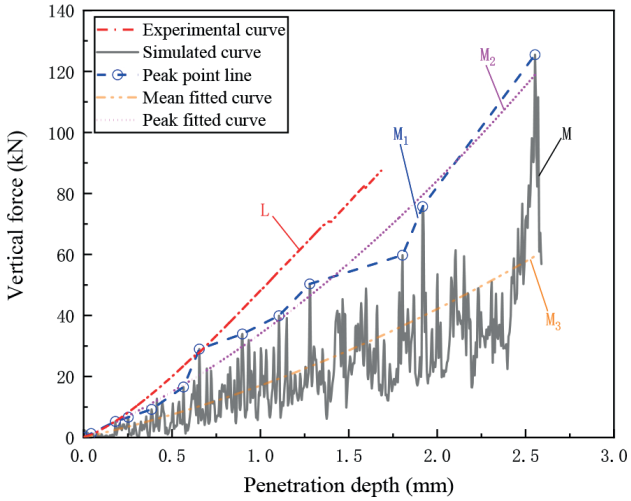

Fig. 18 Comparison of vertical forces obtained by penetration simulation, experiment and fitted values

curve M. It can be seen from the figure that the simulation group reported significantly lower levels of penetration load than the experimental group. Since the dynamic derivation process of the dense core cannot be simulated, the contact stress level is severely underestimated by the simulation. In addition, the time point when the leap-forward breaking occurs in the simulation is earlier than that in the experiment, and multiple leap-forward breaking points can be observed in the simulated curve. The peak fitted curve and the mean fitted curve are used to estimate the prediction accuracy of cutting forces. It can be seen from the figure that the curve M2 is closer to the curve L than curve M3. In other words, the peak point fitting method can better reflect the load characteristics of the disc cutter during the penetration process.

In summary, the penetration model can accurately simulate the rock damage morphology under the action of TBM disc cutters. However, due to the limitations of FEM, the penetration model cannot simulate the dynamic derivation process of the dense core, resulting in underestimation of the load level and load fluctuation degree. The peak point fitting method can be used to reduce the influence of the aforementioned limitations on the prediction accuracy of load level.

6 Feasibility analysis of "step-by-step" modeling

Based on the above accuracy analysis, a novel simulation model of rock penetration by the disc cutter assisted with laser was established, and the feasibility of "step-by-step" modeling method was analyzed by comparing simulation and experimental results.

6.1 Simulation model and experiment preparation

(1) *Model setup*

According to the conclusion of accuracy analysis of laser drilling model in Section 3.2, the laser power in S1 was set to 40 W to reduce the influence of glass glaze on simulation accuracy. Other laser drilling parameters were the same as described in Section 3.1. And then the geometric morphology of the laser hole was predicted by S1. In S2, a FE model of pre-drilled rock with a given cutter-hole distance and hole-hole distance was reconstructed by HyperMesh (cutter-hole distance and hole-hole distance is 4 mm and 2 mm, respectively). In S3, the reconstructed model was imported into the LS-DYNA, and then the simulation model of laser-assisted disc cutter penetration into rock was established, as shown in Fig. 19. The HJC model was also introduced as the constitutive model for rock materials in laser-assisted disc cutter penetration into rock with the same parameters. The details of the boundary conditions were illustrated in Section 5.1.

Based on the apparatus shown in Fig. 3(a), granite specimens were pre-drilled using the same laser parameters as

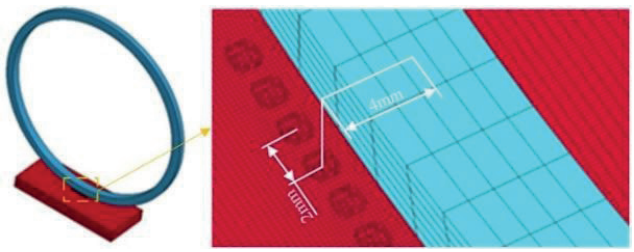

Fig. 19 FE model of Laser-assisted cutter penetration into rock

described in the above simulation. Then, an experimental platform was set up to conduct penetration tests by the disc cutter indenter (see Fig. 15).

6.2 Feasibility analysis

Fig. 20 shows the damage morphology of the rock obtained by the penetration simulation and experiment. It can be observed that the crushed zone initiating below the blade expands outward and extends to the laser holes, generating large rock debris on the side A, which shows that the pre-drilled laser holes has played a leading role in the generation and development of damage. On the side B, only the indentation of the cutter indenter was observed, and the rock damage was not so severe that the damage zone did not expands outward. Obviously, there is a coupling effect between the prefabricated laser holes and the indentation, thereby promoting the intersection of the thermal cracks generated by laser irradiation and the lateral cracks induced by the disc cutter, and then the purpose of improving the rock breaking efficiency of the disc cutter is achieved.

Since the derivation process of the dense core cannot be well simulated, the load level of the simulated vertical force is lower than the experimental results. In order to increase the simulation accuracy, the simulated curves of vertical force with penetration depth were fitted by the peak point fitting method. As shown in Fig. 21, experimental curves without and with pre-drilled laser holes are indexed as X1 and X2, respectively; peak fitted curves of the simulated results without and with pre-drilled laser holes are indexed as Y1 and Y2, respectively. It can be seen from the figure that the trend of fitted vertical forces match well with the experimental results. The vertical forces reflected in curves X2 and Y2 are lower than those in curves X1 and Y1, respectively, which shows that the pre-drilled laser holes can reduce the cutting load of the disc cutter, thereby improving the service life of the tool.

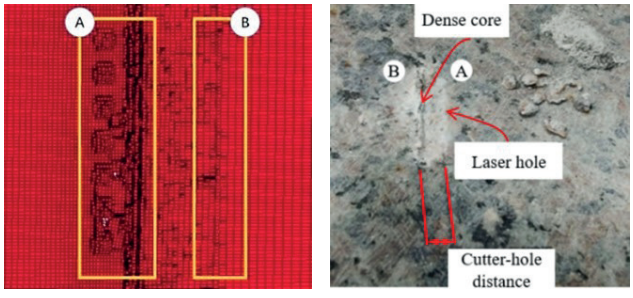

(a) (b)

Fig. 20 Rock damage morphology obtained by laser-assisted indenter penetration: (a) simulated result; (b) experimental result

In summary, rock damage morphology obtained by the simulation as shown in Fig. 20(a) is consistent with the observation of Fig. 20(b). The peak fitted curves illustrates a good agreement with the experimental results. "Step-by-step" modeling method has been proven to have great potential in studying the rock damage mechanism under the action of laser-assisted disc cutters.

7 Conclusions

In order to research the feasibility of laser-assisted disc cutter rock breaking, this paper proposed a "step-by-step" modeling method and discussed the potential influencing factors of simulation accuracy. Suggestions and measures to improve the simulation accuracy of each key step are obtained. Finally, based on the conclusions from accuracy analysis at each step, a simulation model of laser-assisted disc cutter penetration into rock is established, which was proved to be reliable by the rock breaking experiment. The results can provide theoretical guidance and data support for designing the most efficient system of laser-assisted TBM for digging a full-face hard rock tunnel. The details of the conclusions are shown as follows:

1. In the laser drilling simulation (S1), due to the existence of glass glaze, the laser power significantly affects the prediction accuracy of the laser hole, so the results of simulation need to be further corrected when it is popularized and applied under high laser power.
2. In the simulation of rock constitutive behavior (S2), the HJC model can accurately simulate the transient nonlinear fracture behavior of the rock under the action of the existing TBM disc cutters within the given impact velocity range.

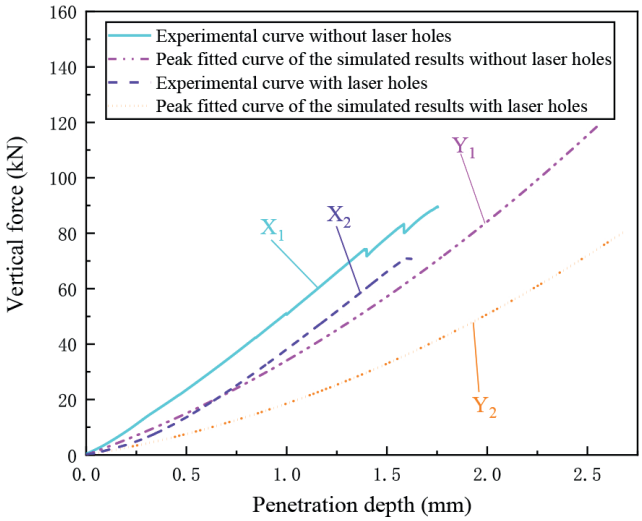

Fig. 21 Comparison of vertical forces obtained by the fitted values and experiments

3. In the simulation of disc cutter penetration (S3), due to the existence of the dense core, the simulated load level is significantly lower than the experimental results, and the peak point fitting method should be introduced to correct the results obtained by the simulation.
4. The "step-by-step" modeling method has high simulation accuracy under certain conditions. In future studies, the influence of the glass glaze and the dense core on simulation accuracy will be implemented in our numerical model.

Acknowledgements

This work was supported by the Science and Technology Innovation Program of Hunan Province (2021RC2094, 2020RC4038, 2020RC2037), the National Natural Science Foundation of China (51704256, 52075465, 11832016) and the Excellent Youth Project of Hunan Provincial Department of Education(22B0127). This work was also supported by National Key Research and Development Program (2021YFB4000800), Hunan Innovative Province Construction Project (2020GK2014), and Hefei General Machinery Research Institute Co., LTD Project (2021ZKKF043). These supports were greatly appreciated.

References

[1] Zhang, X., Liao, Y., Chen, Z., Xia, Y., Zhang, K. "Study on Optimum Free-face Condition of Cutting Hard Rock with Tunnel Boring Machine Hob", Periodica Polytechnica Civil Engineering, 65(2), pp. 501–521, 2021. https://doi.org/10.3311/PPci.17567

[2] Yin, X., Liu, Q., Huang, X., Pan, Y. "Perception model of surrounding rock geological conditions based on TBM operational big data and combined unsupervised-supervised learning", Tunnelling and Underground Space Technology, 120, 104285, 2022. https://doi.org/https://doi.org/10.1016/j.tust.2021.104285

[3] Geng, Q., He, F., Ma, M., Liu, X., Wang, X., Zhang, Z., Ye, M. "Application of Full-Scale Experimental Cutterhead System to Study Penetration Performance of Tunnel Boring Machines (TBMs)", Rock Mechanics and Rock Engineering, 55, pp. 4673–4696, 2022. https://doi.org/10.1007/s00603-022-02886-9

[4] Sabanovic, N., Wannenmacher, H., Stauch, F., Fentzloff, W. "Demands on digital data capturing of TBM and conventional tunnel drives", Geomechanics and Tunnelling, 15(2), pp. 207–214, 2022. https://doi.org/10.1002/geot.202100077

[5] Li, B., Hu, M., Zhang, B., Li, N., Shao, W., Nie, L., Cao, W., Xu, B. "Numerical simulation and experimental studies of rock-breaking methods for pre-grooving-assisted disc cutter", Bulletin of Engineering Geology and the Environment, 81, 90, 2022. https://doi.org/10.1007/s10064-022-02594-2

[6] Cheng, J.-L., Jiang, Z.-H., Han, W.-F., Li, M.-L., Wang, Y.-X. "Breakage mechanism of hard-rock penetration by TBM disc cutter after high pressure water jet precutting", Engineering Fracture Mechanics, 240, 107320, 2020. https://doi.org/10.1016/j.engfracmech.2020.107320

[7] Yao, J., Tao, M., Zhao, R., Hashemi, S. S., Wang, Y. "Effect of microwave treatment on thermal properties and structural degradation of red sandstone in rock excavation", Minerals Engineering, 162, 106730, 2021. https://doi.org/10.1016/j.mineng.2020.106730

[8] Bai, G., Sun, Q., Jia, H., Ge, Z., Li, P. "Variations in fracture toughness of SCB granite influenced by microwave heating", Engineering Fracture Mechanics, 258, 108048, 2021. https://doi.org/10.1016/j.engfracmech.2021.108048

[9] Pan, H., Hu, Y., Kang, Y., Chen, H., Liu, F., Xie, J., Wang, X. "The influence of laser irradiation parameters on thermal breaking characteristics of shale", Journal of Petroleum Science and Engineering, 213, 110397, 2022. https://doi.org/10.1016/j.petrol.2022.110397

[10] Jamali, S., Wittig, V., Börner, J., Bracke, R., Ostendorf, A. "Application of high powered Laser Technology to alter hard rock properties towards lower strength materials for more efficient drilling, mining, and Geothermal Energy production", Geomechanics for Energy and the Environment, 20, 100112, 2019. https://doi.org/10.1016/j.gete.2019.01.001

[11] Zhang, K., Liu, W., Yao, X., Peng, C., Liu, J., Zheng, X. "Investigation on Two-Step Simulation Modeling Method for Rock Breaking by TBM Disc Cutters Assisted with Laser", KSCE Journal of Civil Engineering, 26(6), pp. 2966–2978, 2022. https://doi.org/10.1007/s12205-022-2081-2

[12] Zhang, K., Yang, C., Chen, C., Peng, C., Liu, J. "Scale model test on laser-assisted rock indentation by TBM disc cutter indenter", Rock and Soil Mechanics, 43(01), pp. 87–96, 2022. (in Chinese) https://doi.org/10.16285/j.rsm.2021.0770

[13] Zhang, X., Tan, T., Hu, D., Li, M., Lin, L., Lin, S. "Investigation of Cutting Rock by TBM Hob using a SPG Method", Periodica Polytechnica Civil Engineering, 66(4), pp. 1133–1143, 2022. https://doi.org/10.3311/PPci.20342

[14] Zhang, X., Hu, D., Li, J., Pan, J., Xia, Y., Tian, Y. "Investigation of rock breaking mechanism with TBM hob under traditional and free-face condition", Engineering Fracture Mechanics, 242, 107432, 2021. https://doi.org/10.1016/j.engfracmech.2020.107432

[15] Afrasiabi, N., Rafiee, R., Noroozi, M. "Investigating the effect of discontinuity geometrical parameters on the TBM performance in hard rock", Tunnelling and Underground Space Technology, 84, pp. 326–333, 2019. https://doi.org/10.1016/j.tust.2018.11.039

[16] Xia, Y. M., Guo, B., Cong, G. Q., Zhang, X. H., Zeng, G. Y. "Numerical simulation of rock fragmentation induced by a single TBM disc cutter close to a side free surface", International Journal of Rock Mechanics and Mining Sciences, 91, pp. 40–48, 2017. https://doi.org/10.1016/j.ijrmms.2016.11.004

[17] Qin, Y., Förster, D. J., Weber, R., Graf, T., Yang, S. "Numerical study of the dynamics of the hole formation during drilling with combined ms and ns laser pulses", Optics and Laser Technology, 112, pp. 8–19, 2019.
https://doi.org/10.1016/j.optlastec.2018.10.057

[18] Chen, K., Huang, Z., Deng, R., Zhang, W., Kang, M., Ma, Y., Shi, M., Yan, J. "Research on the temperature and stress fields of elliptical laser irradiated sandstone, and drilling with the elliptical laser-assisted mechanical bit", Journal of Petroleum Science and Engineering, 211, 110147, 2022.
https://doi.org/10.1016/j.petrol.2022.110147

[19] Chen, K., Huang, Z., Deng, R., Zhang, W., Kang, M., Ma, Y. "Numerical Simulation and Test Investigation on Phase Transition and Thermal Cracking Process of Sandstone by Laser Drilling", Rock Mechanics and Rock Engineering, 55, pp. 2129–2147, 2022.
https://doi.org/10.1007/s00603-021-02764-w

[20] Li, M., Han, B., Zhang, S., Song, L., He, Q. "Numerical simulation and experimental investigation on fracture mechanism of granite by laser irradiation", Optics and Laser Technology, 106, pp. 52–60, 2018.
https://doi.org/10.1016/j.optlastec.2018.03.016

[21] Shugaev, M. V., He, M., Levy, Y., Mazzi, A., Miotello, A., Bulgakova, N. M., Zhigilei, L. V. "Laser-induced thermal processes: heat transfer, generation of stresses, melting and solidification, vaporization, and phase explosion", In: Sugioka, K. (ed.) Handbook of Laser Micro-and Nano-Engineering, Springer International Publishing, 2021, pp. 83–163. ISBN 978-3-030-63646-3
https://doi.org/10.1007/978-3-030-63647-0_11

[22] Yang, X., Zhou, X., Zhu, H., Zhou, J., Li, Y. "Experimental Investigation on Hard Rock Breaking with Fiber Laser: Surface Failure Characteristics and Perforating Mechanism", Advances in Civil Engineering, 2020, 1316796, 2020.
https://doi.org/10.1155/2020/1316796

[23] Rui, F., Zhao, G.-F. "Experimental and numerical investigation of laser-induced rock damage and the implications for laser-assisted rock cutting", International Journal of Rock Mechanics and Mining Sciences, 139, 104653, 2021.
https://doi.org/10.1016/j.ijrmms.2021.104653

[24] Wang, Z., Wang, H., Wang, J., Tian, N. "Finite element analyses of constitutive models performance in the simulation of blast-induced rock cracks", Computers and Geotechnics, 135, 104172, 2021.
https://doi.org/10.1016/j.compgeo.2021.104172

[25] Wan, W., Yang, J., Xu, G., Liu, Y. "Determination and evaluation of Holmquist-Johnson-Cook constitutive model parameters for ultra-high-performance concrete with steel fibers", International Journal of Impact Engineering, 156, 103966, 2021.
https://doi.org/10.1016/j.ijimpeng.2021.103966

[26] Zhao, Y., Bi, J., Zhou, X.-P. "Quantitative analysis of rockburst in the surrounding rock masses around deep tunnels", Engineering Geology, 273, 105669, 2020.
https://doi.org/10.1016/j.enggeo.2020.105669

[27] Lv, T. H., Chen, X. W., Chen, G. "The 3D meso-scale model and numerical tests of split Hopkinson pressure bar of concrete specimen", Construction and Building Materials, 160, pp. 744–764, 2018.
https://doi.org/10.1016/j.conbuildmat.2017.11.094

[28] Du, Y., Wei, J., Liu, K., Huang, D., Lin, Q., Yang, B. "Research on dynamic constitutive model of ultra-high performance fiber-reinforced concrete", Construction and Building Materials, 234, 117386, 2020.
https://doi.org/10.1016/j.conbuildmat.2019.117386

[29] Yang, L., Xu, W., Yilmaz, E., Wang, Q., Qiu, J. "A combined experimental and numerical study on the triaxial and dynamic compression behavior of cemented tailings backfill", Engineering Structures, 219, 110957, 2020.
https://doi.org/10.1016/j.engstruct.2020.110957